RESEARCH

Slow Magnetoacoustic Waves in Smoothly Nonuniform Coronal Plasma Structures

Viktor V. Fedenev[1] (ORCID) · **Valery M. Nakariakov[2,3]** (ORCID) · **Sergey A. Anfinogentov[1]** (ORCID)

Abstract

Numerical simulations of a propagating slow magnetoacoustic wave guided by a field-aligned low-β plasma nonuniformity are performed in terms of ideal magnetohydrodynamics, aiming at modeling propagating extreme ultraviolet (EUV) emission disturbances observed in the solar corona. The perpendicular profiles of the equilibrium density and temperature are smoothly nonuniform, resulting in smoothly nonuniform profiles of the sound and tube speeds. It is found that an initially plane wavefront perpendicular to the magnetic field experiences a growing deformation with the distance from the driver. The segments of the wavefront located at higher sound speed regions propagate along the field faster. This results in progressively increasing phase mixing. At some distance from the wave driver, at a certain perpendicular cross-section of the nonuniformity, there are opposite phases of the wave. As local perpendicular phase and group speeds are opposite to each other, the slow wave energy tends towards regions of the higher local sound speed. This effect increases with the increase in the plasma-β. Thus, plasma nonuniformities with temperature decreases are slow magnetoacoustic anti-waveguides, while those with temperature increases are waveguides. In the optically thin radiation regime, typical for the EUV emission from the solar corona, phase mixing of slow waves leads to apparent damping of the waves. This damping is not connected with any dissipative process, and is caused by the destructive interference of slow perturbations with different phases, integrated along the line of sight. The apparent damping depends on the combination of magnetic-field strengths, plasma-β, and viewing angles. This effect could be responsible for nonsystematic dependencies of the damping length upon the oscillation periods and the plasma temperature, appearing in observations.

Keywords Waves, Magnetohydrodynamic · Waves, Propagation · Corona, Structures

✉ V.V. Fedenev
    fedenev@iszf.irk.ru

  V.M. Nakariakov
  vnakariakov@googlemail.com

  S.A. Anfinogentov
  anfinogentov@iszf.irk.ru

[1] Institute of Solar-Terrestrial Physics (ISZF), Lermontov st., 126a, Irkutsk, 664033 Russia

[2] Centro de Investigación en Astronomía, Universidad Bernardo O'Higgins, Avenida Viel 1497, Santiago, 8370993, Chile

[3] Saint Petersburg Branch, Special Astrophysical Observatory of RAS, Saint Petersburg 196140, Russia

1. Introduction

Slow magnetoacoustic waves are among the most studied magnetohydrodynamic (MHD) wave modes in the solar corona (e.g., Nakariakov and Kolotkov, 2020). Coronal slow waves are observed in two regimes. Standing slow oscillations are typically detected as rapidly decaying oscillations of Doppler shifts of coronal extreme ultraviolet (EUV) emission lines formed in hot coronal loops (see Wang et al., 2021, for a recent comprehensive review). In imaging observations, the emission intensity is often seen to bounce back and forth between the loop's footpoints (e.g., Kumar, Innes, and Inhester, 2013), i.e., the waves are sloshing, which suggests a co-existence of several parallel standing harmonics (Nakariakov et al., 2019). The other regime is demonstrated by propagating EUV brightness disturbances in open magnetic structures such as plumes in polar regions (e.g., DeForest and Gurman, 1998; Nakariakov, 2006) and coronal fan structures associated with sunspots (Berghmans and Clette, 1999; De Moortel et al., 2002b). Propagating slow waves have a bias towards enhancement of the intensity in the blue wing of the emission line, which sometimes caused an erroneous interpretation of this phenomenon as periodic plasma flows. However, in a low-β coronal plasma, the blue-wing asymmetry is an inherent property of a slow wave propagating towards the observer because of the intrinsic in-phase behavior of velocity and density perturbations (Verwichte et al., 2010); see also (Wang et al., 2009). The main difference between sloshing and propagating slow waves is the lack of reflection in the latter case. Propagating slow waves observed in fan structures and plumes share similar properties; see Banerjee et al. (2021) for a recent review. It is still unclear whether the periodic compressive perturbations observed in the white light at much larger heights, for example, the 9-min oscillations detected at 1.9 $R_\odot$ by Ofman et al. (1997) and the 7 – 8 min oscillations detected at 1.5 – 2.2 $R_\odot$ by Morgan, Habbal, and Li (2004), are of the same nature as the propagating EUV disturbances in fans and plumes.

Typical apparent phase speeds of coronal slow waves are sub-sonic, which corresponds to the propagation at the sound speed reduced by the projection effect. A quasi-stereoscopic observation of a coronal slow wave confirmed its propagation at the local sound speed determined by the plasma temperature (Marsh et al., 2003). The phase speed increases with the temperature (e.g., Su, 2014). Typical oscillation periods are from a few to several minutes. The periods are likely determined by characteristic periods of chromospheric oscillations at the footpoints of the waveguiding structures (e.g., Sych et al., 2009; Botha et al., 2011; Kobanov, Kolobov, and Chelpanov, 2015). An important feature of propagating slow waves is a rapid decay with height, typically within 10 Mm, e.g., 8.9 ± 4.4 Mm as estimated in De Moortel et al. (2002a). Sometimes, the waves are detected to reach larger distances from the solar surface, for example, 20 Mm (Marsh, De Moortel, and Walsh, 2011). The empirical dependence of the damping length on the oscillation period is puzzling, as in different observations it either increases or decreases with an increase in the period (e.g., Krishna Prasad et al., 2012; Krishna Prasad, Banerjee, and Van Doorsselaere, 2014; Mandal, Krishna Prasad, and Banerjee, 2018). The dependence of the damping length on the plasma temperature in the waveguiding plasma structure is not systematic either (Krishna Prasad, Jess, and Van Doorsselaere, 2019).

Theoretical modeling of coronal slow waves is generally based upon three approaches. The simplest model is the infinite field approximation in which effects of finite plasma-β are neglected ($\beta = 0$), and the description reduces to one-dimensional acoustic equations (e.g., Nakariakov et al., 2000). A more elaborated 1D model which allows for finite-β effects is the thin flux tube approximation (e.g., Roberts and Webb, 1978) based on the assumption that the parallel wavelength of the wave is much greater than the perpendicular size of the

waveguide. The second-order generalization of the thin flux tube approximation includes effects of the finite perpendicular cross-section and the magnetic-field twist (e.g., Zhugzhda, 1996; Zhugzhda and Goossens, 2001). A more advanced model which accounts for the perpendicular structure of the perturbations considers a waveguiding plasma nonuniformity as a plasma slab or cylinder with constant plasma parameters, surrounded with a plasma with different parameters which are constant too (e.g., Roberts, 1981; Edwin and Roberts, 1983). Under coronal conditions, the phase speed of slow magnetoacoustic waves guided by the nonuniformity is between the values of the sound speed and the tube (cusp) speed determined by the sound and Alfvén speeds. The speeds are determined by the plasma parameters inside the waveguide. Full-scale MHD modeling of propagating slow magnetoacoustic waves guided by a coronal plasma nonuniformity has been performed by, for example, Ofman, Nakariakov, and DeForest (1999), Selwa, Murawski, and Solanki (2005).

The observed rapid damping of propagating slow waves stimulated a number of dedicated studies which associated this effect either with enhanced thermal conduction along the magnetic field, with effects of compressive viscosity, radiation, density stratification, and the divergence of the waveguiding plasma structure with height (e.g., De Moortel and Hood, 2003, 2004; Owen, De Moortel, and Hood, 2009; Marsh, De Moortel, and Walsh, 2011), or with the back-reaction of the wave-induced misbalance of the coronal heating and cooling processes (Kolotkov, Nakariakov, and Zavershinskii, 2019). Another mechanism for the apparent damping of coronal propagating slow waves is connected with the deformation of the wavefront by the nonuniformity of the plasma temperature in the perpendicular direction (Voitenko et al., 2005). This mechanism is based on the confinement of the slow wave propagation to the direction of the magnetic field. With the decrease in plasma-β, a slow wave propagates at a progressively narrow angle to the field. If the sound speed is nonuniform across the field, the waves propagate almost along specific field lines at the local sound speeds. This effect causes the increase in the perpendicular wave number, and hence the enhanced dissipation by the mechanisms which depend on the wave number, i.e., the viscosity, thermal conduction, and resistivity. This effect is similar to the effect of Alfvén wave phase mixing in a perpendicularly nonuniform plasma, proposed by Heyvaerts and Priest (1983).

Coronal slow wave models must also account for the specific dependence of the observed perturbations of the EUV emission intensity on the plasma parameters perturbed by the wave, e.g., the plasma density and temperature. Forward modeling of propagating EUV disturbances associated with coronal slow waves has demonstrated certain inconsistencies between the observed and actual parameters of the waves, in particular the damping time (De Moortel and Bradshaw, 2008). On the other hand, forward modeling performed by Mandal et al. (2016) showed that the theoretical dependence of the damping length on wave periods is consistent with the results of numerical modeling and observations. In particular, that study accounted for the effects of the oblique line-of-sight (LoS) angle, optically thin column depth, and finite pixel size (see, e.g., Cooper, Nakariakov, and Tsiklauri, 2003), while the perpendicular profile of the sound speed was taken to be almost step-like. The latter assumption did not allow to see the effect of phase mixing on the apparent wave damping caused by the appearance of positive and negative phases of the wave perturbation along the LoS. However, the importance of phase mixing has been demonstrated by Voitenko et al. (2005), who consider a linear perpendicular profile of the plasma temperature, i.e., in the absence of a waveguide. The LoS was taken in the direction perpendicular to the magnetic field. An observational justification of the need for considering fine perpendicular structuring of the corona, i.e., its multi-thermal multi-stranded nature, is provided by analyses of multi-wavelength observations (e.g., Brooks, Warren, and Ugarte-Urra, 2012; Schmelz, Christian, and Chastain, 2016) and by seismological estimations (e.g., Van Doorsselaere et al., 2008), and it is also predicted theoretically (e.g., Williams et al., 2021).

The aim of this paper is to study the propagation of a linear slow magnetoacoustic wave in a field-aligned low-β plasma slab in terms of ideal MHD. Profiles of the equilibrium plasma temperature, density, and magnetic-field strength across the magnetic field are smooth and have an extreme at the axis of the waveguide. Slabs with both increased and decreased temperatures are considered. Attention is also paid to the observational manifestation of the apparent wave damping because of phase mixing. In Section 2 we describe the numerical approach and the model setup. In Section 3 we apply the local approximation and demonstrate that perpendicular phase and group speeds of slow magnetoacoustic waves are opposite to each other. Numerical results obtained are presented in Section 4 and discussed in Section 5.

2. Numerical Approach

2.1. Computational Setup

In this work we study the dynamics of slow magnetoacoustic waves numerically. Simulations were performed using the LareND numerical code (Arber et al., 2001), which is a staggered grid MHD code created to simulate the evolution of low-β plasma systems in Cartesian geometry. To ensure the stability of the numerical scheme, the code uses a dynamic time step with a predictor defined by the Courant–Friedrichs–Lewy condition, setting the Courant number to less than or equal to 1.

In this study we used Lare2D – a two-dimensional version of this code. It renders all physical quantities constant along a specified axis to reduce computation time for simple problems. The coronal medium is modeled as a fully ionized plasma with the equation of state of ideal gas. Radiation losses, thermal conduction, viscosity and resistivity, and coronal heating are turned off. The set of ideal MHD equations solved in our study is

$$\frac{\partial \rho}{\partial t} = -\nabla \cdot (\rho \mathbf{v}),$$

$$\rho \frac{D\mathbf{v}}{Dt} = \mathbf{j} \times \mathbf{B} - \nabla P,$$

$$\frac{\partial \mathbf{B}}{\partial t} = -\nabla \times \mathbf{E},$$

$$\frac{D\epsilon}{Dt} + \frac{P}{\rho} \nabla \cdot \mathbf{v} = 0, \tag{1}$$

$$\mathbf{E} + \mathbf{v} \times \mathbf{B} = 0,$$

$$\nabla \times \mathbf{B} = \mu_0 \mathbf{j},$$

$$P = \frac{\rho k_B T}{\mu_m},$$

$$\epsilon = \frac{P}{\rho(\gamma - 1)} = \frac{k_B T}{\mu_m(\gamma - 1)},$$

where the variables ρ, P, ϵ, T, $\mathbf{v}$, $\mathbf{B}$, $\mathbf{j}$, and $\mathbf{E}$ are the mass density, gas pressure, specific internal energy density, temperature, plasma bulk velocity, magnetic field, electric current, and electric field, respectively, μ_0 is the magnetic permeability of vacuum, μ_m is the mean particle mass, $\gamma = 5/3$ is the adiabatic index, and the capital D denotes the total derivative.
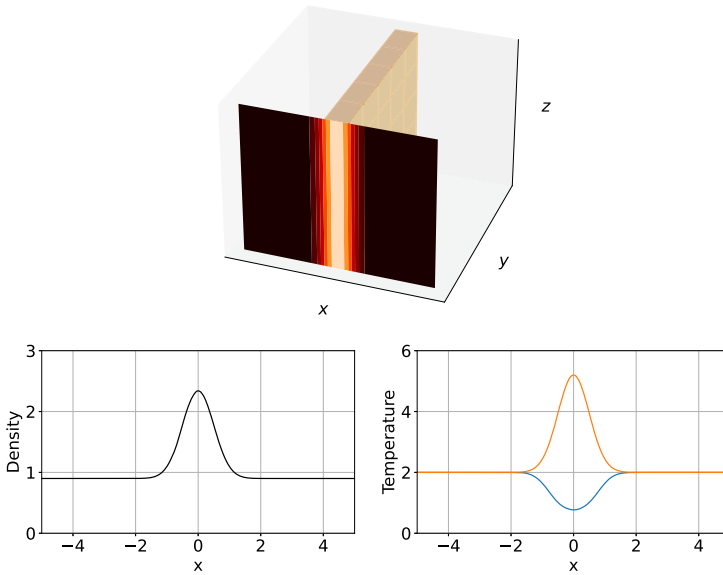
Figure 1 Geometry of the model. Top panel: The smooth plasma nonuniformity stretched along the magnetic field. The equilibrium magnetic field is in the z-direction, and all variables are constant in the y-direction. Bottom panels: Equilibrium mass density (left) and temperature (right) profiles in the perpendicular, x-direction. The red and blue curves show hot and cool plasma slabs, respectively.

Equations 1 are solved in a box consisting of 512×2048 cells, on the interval $[-5, 5]$ on the x-axis and the interval $[0, 40]$ on the z-axis, with arbitrary units. Thus, the size of the computational domain is 10×40 arbitrary units.

Boundary conditions on the top, left, and right sides of the box are set up as reflective. The wave driver is located at the lower boundary and launches waves by varying the vertical component of the velocity. Such a driver launches almost pure slow magnetoacoustic waves traveling upward along the magnetic-field lines. The simulation is stopped before the waves reach the top boundary to avoid interference of the upward traveling waves with those reflected from the top boundary.

2.2. Model Setup

We model a waveguiding field-aligned plasma nonuniformity of the solar corona as a plasma slab stretched along the equilibrium magnetic field in the z-direction, with the equilibrium profiles of the plasma density and temperature across the field, in the x-direction. Thus, we neglect the effects of the magnetic-field curvature and gravitational stratification. In the low-β plasma typical for the corona, the use of Cartesian geometry instead of cylindrical geometry is not expected to have a noticeable impact on the properties of slow magnetoacoustic waves (e.g., Roberts, 1981; Edwin and Roberts, 1983). We consider cases of both warm and cool slabs, with the temperature inside the slab being higher and lower, respectively, than outside it. The geometry of the model is shown in Figure 1.

The equilibrium density profile is set as

$$\rho_0(x) = \rho_\infty \left[1 + m \exp\left(-\frac{x^2}{2\sigma^2} \right) \right], \tag{2}$$
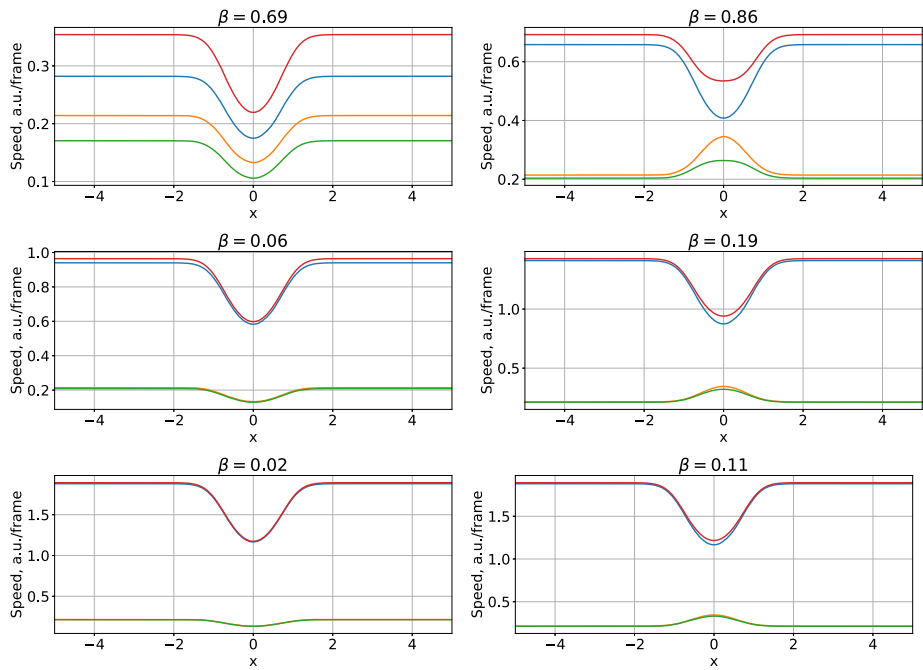
Figure 2 Equilibrium profiles of the Alfvén (C_A, blue), sound (C_s, orange), tube (C_t, green), and fast (C_f, red) speeds across the plasma slab for different values of the plasma-β at the slab's center. The left and right columns show cool and warm plasma slabs, respectively. The units are arbitrary. In the left bottom panel the orange and green curves practically coincide.

where ρ_∞ is the background density far from the slab, $m = 1.6$ is the density contrast parameter, and $\sigma = 0.5$ is the characteristic width of the slab. The spatial parameters are given in arbitrary units. The equilibrium magnetic field $\mathbf{B}_0 = (0, 0, B_{z0})$ is straight. Gravity is neglected. The total pressure balance in equilibrium is achieved by balancing the equilibrium density, temperature, and the magnetic-field profiles to keep the total pressure constant at every location in the computational domain. In the case of a cool plasma slab, the magnetic field is kept constant and the pressure balance is achieved by varying only the density and temperature, while the model of a warm slab requires variations of the magnetic-field strength to balance the variation of the plasma pressure increase within the slab. Typical equilibrium profiles of the density and temperature are shown in the bottom row of Figure 1. The equilibrium values of the magnetic field B_{z0}, density ρ_0, and temperature T_0 determine characteristic speeds of MHD wave dynamics in the system, such as the Alfvén speed $C_A = B_{z0}/(\mu\rho_0)^{1/2}$ and the sound speed $C_s = (\gamma k_B T_0/\mu_m)^{1/2}$. Two other characteristic speeds, the fast speed $C_f = (C_A^2 + C_s^2)^{1/2}$ and the tube (or cusp) speed $C_t = C_s C_A/(C_s^2 + C_A^2)^{1/2}$, are determined by the values of the Alfvén and sound speeds. The corresponding profiles of characteristic speeds across the slab, considered in our study, are given in Figure 2. The equilibrium values of the plasma-β are selected to cover the range typical for solar coronal and chromospheric plasmas, from 0.02 to 0.86.

Figure 3 Dependence of perpendicular components of the phase (red) and group (blue) velocities upon the perpendicular wave number for the parallel wave number $k_z = 1$, in a uniform medium with Alfvén speed $C_A = 1.5$ and sound speed $C_s = 1$.
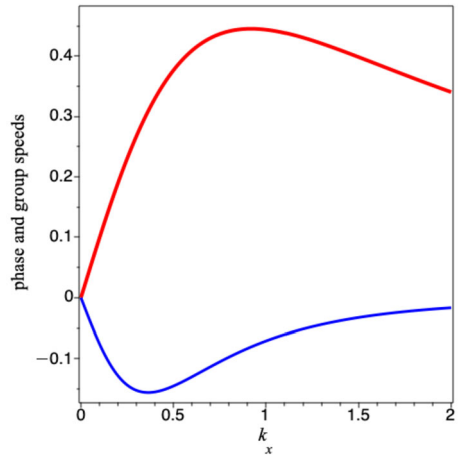
At the bottom of the computational domain, $z = 0$, the vertical component of the plasma velocity is set to oscillate harmonically in time,

$$V_z(x, 0) = A_0 \exp\left[-\frac{1}{2}\left(\frac{x}{\sigma}\right)^8 \right] \sin(\omega t), \tag{3}$$

where $A_0 = 0.01 C_s(x = 0)$ is the amplitude of the driver. The value of the amplitude was chosen to be small to prevent the formation of shock waves and other nonlinear effects. The period of the driver was set to $\omega = 0.035$ arbitrary units, which corresponds to 18 computational time steps. In a low-β plasma such a driver excites mainly slow magnetoacoustic waves which propagate in the z-direction. Initially, slow wavefronts are parallel to the x-axis, i.e., perpendicular to the field and the axis of the slab.

3. Theory: Local Approximation

It is instructive to begin with recalling that perpendicular phase and group speeds of slow magnetoacoustic waves are opposite to each other. Consider a uniform equilibrium with constant Alfvén and sound speeds, i.e., neglecting the perpendicular nonuniformity. The dispersion relation of linear slow magnetoacoustic waves, linking the circular frequency ω and parallel and perpendicular components of the wave vector, k_z and k_x, respectively, is

$$\omega^2 = \frac{1}{2}\Big[(C_A^2 + C_s^2)(k_x^2 + k_z^2) \tag{4}$$

$$-\sqrt{(C_A^2 + C_s^2)^2(k_x^2 + k_z^2)^2 - 4C_s^2 C_A^2 k_z^2(k_x^2 + k_z^2)}\Big]$$

(see, e.g., Goedbloed and Poedts, 2004; Nakariakov and Zimovets, 2011). The dependence of the perpendicular component of the phase velocity $(\omega/k)(k_x/k)$, where $k = (k_x^2 + k_z^2)^{1/2}$ (Li et al., 2023), and the group speed $d\omega/dk_x$ on the perpendicular wave number k_x is shown in Figure 3. It is evident that the signs of the speeds are opposite. In a nonuniform medium, one would expect that turning of the wave vector towards the region with a low sound speed is accompanied by energy transfer in the opposite direction.

Figure 4 Perturbations of the density in a slow magnetoacoustic wave in a plasma slab with a decrease in the equilibrium plasma temperature (left panel, at $t = 230$, for $\beta = 0.69$) and with an increase in the equilibrium plasma temperature (right panel, at $t = 100$, for $\beta = 0.11$). The unperturbed background is subtracted from the images, and the residual density perturbation is normalized to its maximum.
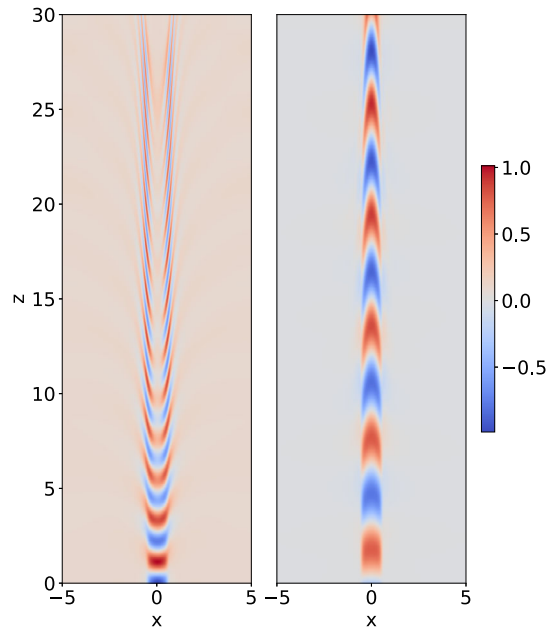
4. Numerical Results

4.1. Phase Mixing and Refraction

Numerical solutions of the set of MHD equations 1 supplemented with boundary condition 3 demonstrated the evolution of the plasma variables in the computational domain (x, z). In the context of the research topic, we observe slow magnetoacoustic waves propagating upwards from the bottom of the slab (Figure 4). Because of the nonuniformity of the sound and tube speeds across the field, slow waves experience phase mixing. Specifically, the segments of the wavefront located at higher sound speeds propagate along the magnetic field faster. At the same distance from the driver, wave perturbations situated at different magnetic surfaces defined by different values of the perpendicular coordinate x gradually become out of phase with each other. This effect is also manifested by gradual turning of the initially perpendicular wavefronts towards the regions with a decrease in the sound and tube speeds. With the distance from the source, in the z-direction, the wavefronts become highly oblique in the regions with the highest gradients of the sound and tube speeds (see Figure 4). For the symmetric perpendicular profiles of the plasma temperature, the initially plane wavefronts obtain a horseshoe shape (which can also be called a "chevron" shape) with the distance from the driver. This effect occurs for all values of the plasma-β.

Figures 5 and 6 show the redistribution of the slow wave energy in the waveguiding slab. In a slab with a local decrease in plasma temperature, the local wave vector which is initially directed along the equilibrium field, in the z-direction, turns towards the center of the waveguide (Figure 5). However, as in a slow wave the perpendicular components of the group and phase velocities are directed in the opposite directions (see Section 3), the energy propagates outside the slab. Thus, at some distance from the driver, the slow wave energy leaves the waveguide. In other words, a slab with a decrease in plasma temperature acts as an anti-waveguide for slow waves. The dependence of the wave energy density along a chosen
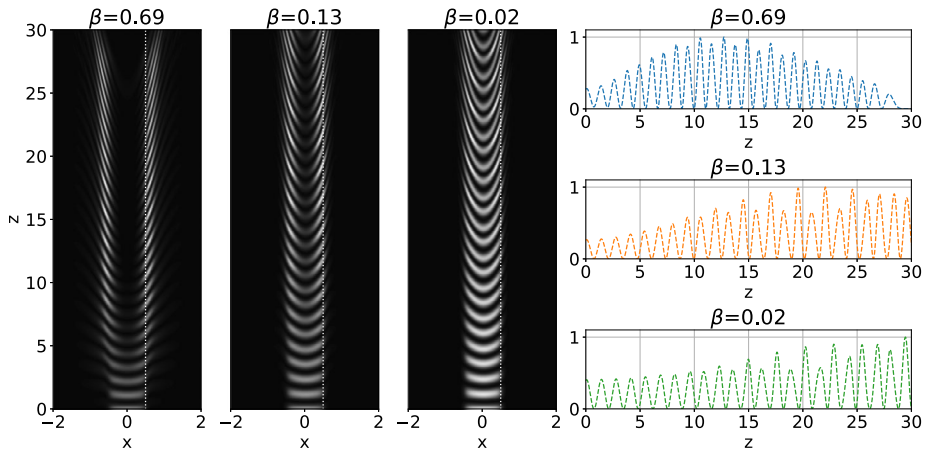
Figure 5 Redistribution of the slow magnetoacoustic wave energy in a cool plasma slab. The gray-scale plots show snapshots of the kinetic energy density $(\rho v^2/2)(x, z)$ in the wave at $t = 230$ arbitrary units in equilibria with different values of the plasma-β. The right column shows the evolution of the energy density with the distance from the driver at the distance $x = 0.5$ from the axis of the slab, indicated by the white dotted line in the panels on the left. The oscillatory signals are normalized to the largest amplitude. The corresponding values of the plasma-β are indicated in the tops of the panels.
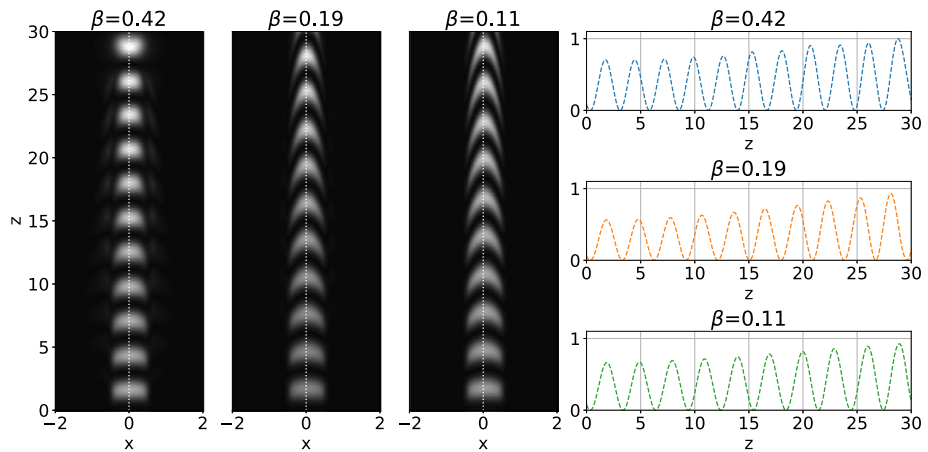

Figure 6 Same as in Figure 5, but for a warm slab at $t = 100$. In the right column, the evolution of the wave energy density with the distance from the driver is shown for the center of the slab, indicated by the white dotted line in the panels on the left.

magnetic surface is not constant. The evolution of the slow wave energy density at a certain location from the center of the slab with the distance from the driver is demonstrated in the right panel of Figure 5. We see that initially the local energy increases, because of the refraction from the center of the slab. At larger distances, the energy may experience a decrease, as the wave leaves this magnetic surface. The decrease in the local energy density is not connected with phase mixing, as, for example, Figure 5 shows that the energy density decreases in the vicinity of $x = 0$ where phase mixing is absent. The effect of refraction is more pronounced for larger values of the plasma-β, when the slow waves are more "oblique." The

effect of refraction disappears when β goes to zero, i.e., when the plasma flows in the wave are almost parallel to the equilibrium field. In particular, this finding justifies the use of the infinite field approximation in the consideration of coronal slow waves.

The behavior of a slow wave in a slab with a local increase in plasma temperature is different from the case of a cool plasma slab (see Figure 6). Similarly to the cool slab case, the smooth perpendicular nonuniformity of the plasma temperature causes the deformation of the wavefronts, and hence phase mixing. However, in this case, because of the refraction, the wave energy gradually concentrates at the axis of the slab.

4.2. Apparent Damping

The perturbations of the plasma density and temperature in coronal slow magnetoacoustic waves cause perturbations of the optically thin emission intensity in the EUV band. The emission intensity I can be estimated by integrating the product of the density squared and the instrument-specific contribution function $G(\lambda, \rho, T)$, where λ is the wavelength of the observational passband, along the LoS (e.g., Van Doorsselaere et al., 2016):

$$I = \int_{(LoS)} \rho^2 G(\lambda, \rho, T) dl. \tag{5}$$

If the wave experiences phase mixing, the resulting intensity perturbation may be affected by constructive or destructive interference of local increases and decreases in, for example, the plasma density in different segments of the integration path. We studied this effect by choosing the contribution function to be a Gaussian (in the logarithmic temperature scale) centered at the slab core temperature. Its width matches the width of the temperature response function of the 171 Å channel of SDO/AIA, provided by the AIA package of SolarSoft (Freeland and Handy, 1998). Assuming the LoS to be straight, we estimated the perturbations of the EUV emission intensity caused by a slow magnetoacoustic wave guided by a plasma slab for several angles between the slab and the LoS situated in the plane (x, z) (Figure 7). The input perturbations of MHD parameters in the slab are described in Section 4.1. An important feature of this estimation is that there could be both local increases and decreases in the plasma density along the LoS. Hence the emission intensity is affected by the superposition of those signals. At small distances from the driver, this effect comes into play for narrow observational angles, while at larger distances this effect appears for all angles because of phase mixing.

Snapshots of the forward modeled variation of the optically thin emission intensity for various LoS angles are shown in Figure 8. Following a brief transition phase, the intensity variations have an oscillatory structure. As expected, the wavelength increases with the increase in the temperature inside the slab for a fixed frequency of the driver. The amplitude of the intensity variations decreases with the distance from the driver. This decrease is apparent, as our simulations are performed in terms of ideal MHD, and the numerical dissipation is not pronounced. The apparent damping is sensitive to the plasma parameter β and the viewing angle.

5. Discussion and Conclusions

We numerically modeled the evolution of slow magnetoacoustic waves in a plasma slab with a smooth nonuniformity of the plasma parameters, stretched along a straight magnetic

Figure 7 Snapshots of the EUV emissivity modulated by phase-mixed slow magnetoacoustic waves, in the waveguiding plasma slab. The arrows show various lines of sight chosen for the integration. The unperturbed background is subtracted from the image. Slabs with the decrease and increase in the plasma temperature are shown in the left ($\beta = 0.69$, $t = 230$) and right ($\beta = 0.19$, $t = 100$) panels, respectively.
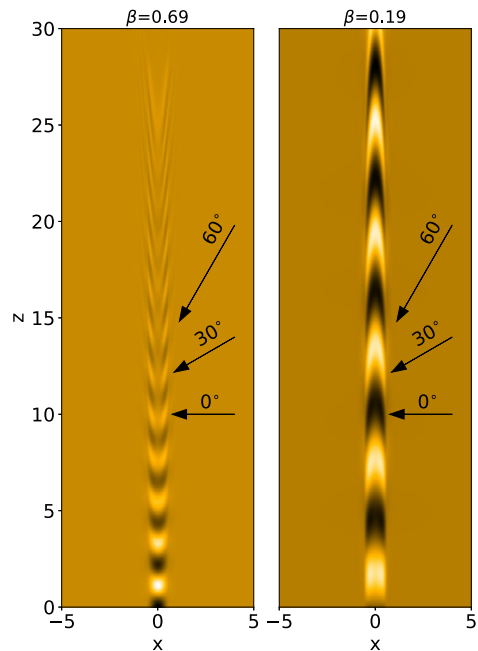
field. Such an equilibrium resembles typical coronal structures which guide propagating disturbances of the EUV emission, such as fan-like structures over sunspots and plumes in coronal holes. The modeling was carried out in terms of ideal MHD, i.e. dissipative and thermal misbalance effects were neglected. The plasma was taken to be of low β. Both cases of the slabs with increased and decreased temperatures in the slab, corresponding to increases and decreases in the local sound speed, respectively, were considered. The model is two-dimensional, addressing motions in the plane formed by the magnetic-field direction and the gradient of the equilibrium plasma parameters. The waves were excited by harmonic field-aligned movements of the footpoint. Such a driver mimics, for example, 3-min oscillations in sunspot umbrae or in pores. The initial wavefront is plane and perpendicular to the magnetic field.

Vertical movements of the footpoint were found to result in slow magnetoacoustic waves propagating mainly upwards. The perpendicular nonuniformity of the sound speed causes the deformation of the wavefronts, which becomes more pronounced with the distance from the driver. As the considered temperature profiles are symmetric with respect to the axis of the slab, the deformed wavefronts have a horseshoe shape. The horseshoe is either convex or concave, depending on whether there is an increase or decrease in the sound speed at the axis of the slab. Such a deformation of the wavefront shape resembles the effect of phase mixing, usually discussed in association with Alfvén waves (e.g., Heyvaerts and Priest, 1983). Similarly to Alfvén waves, the effect of phase mixing progressively increases the nonuniformity of the wavefronts in the perpendicular direction. In other words, the phase speed becomes progressively oblique with the distance from the driver. This process leads to the gradual energy transfer towards smaller perpendicular spatial scales in the wave, which increases the wave damping by the shear viscosity and electrical resistivity. Moreover, as has been pointed out by Voitenko et al. (2005), in the optically thin regime, it may lead to the apparent damping of the observed waves because of the destructive interference. We confirmed the latter by forward modeling of the emission intensity variation along the slab,
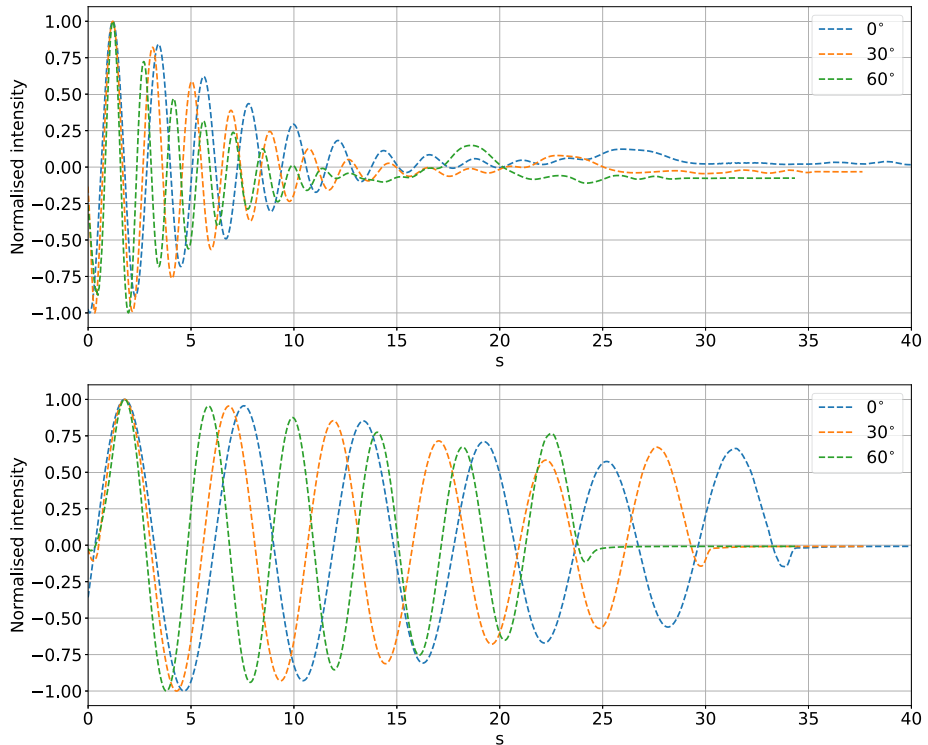
Figure 8 Snapshots of the forward-modeled optically thin EUV intensity variations in a plasma slab, caused by guided slow magnetoacoustic waves. The horizontal axis represents the apparent distance along the slab in the plane of the sky, seen from different viewing angles. Slabs with a decrease and increase in the plasma temperature are shown in the top ($\beta = 0.69$, $t = 230$) and bottom ($\beta = 0.11$, $t = 100$) panels, respectively.

observed with different viewing angles. Thus, the effect of apparent damping of coronal slow waves by phase mixing could be responsible for the nonsystematic dependence of the damping length on oscillation periods and plasma temperature, appearing in observations (e.g., Krishna Prasad et al., 2012; Krishna Prasad, Banerjee, and Van Doorsselaere, 2014; Mandal, Krishna Prasad, and Banerjee, 2018; Krishna Prasad, Jess, and Van Doorsselaere, 2019). Furthermore, the effectiveness of the apparent damping is determined by the speed of phase mixing, which is determined by the perpendicular profile of the plasma temperature. Thus, this effect could be used for probing fine, sub-resolution structuring of the coronal temperature across the magnetic field.

Because of the finite value of the plasma parameter β, the excited slow waves propagate in the perpendicular direction too. It was found that in contrast to fast magnetoacoustic waves which experience refraction towards the regions with the local decrease in the fast speed (e.g., Edwin and Roberts, 1988; Pascoe, Nakariakov, and Kupriyanova, 2014), slow waves experience "anti-refraction" towards the regions with the increase in the sound (or tube) speed. Wavefronts of slow waves turn towards the regions with the low sound speed, in the direction of the phase velocity. However, in the perpendicular direction, the slow wave energy flux characterized by the group velocity is anti-parallel to the phase velocity, which is demonstrated by the local approximation. Thus, the wave energy gradually leaves the region of the lower sound speed towards regions with the higher sound speed, with the distance

from the driver. In other words, field-aligned plasma slabs with an increase in temperature are slow magnetoacoustic waveguides, while the slabs with a temperature decrease are anti-waveguides. This effect increases with the increase in plasma-β.

Declarations

Competing interests The authors declare no competing interests.

References

Arber, T.D., Longbottom, A.W., Gerrard, C.L., Milne, A.M.: 2001, A Staggered Grid, Lagrangian-Eulerian Remap Code for 3-D MHD Simulations. *J. Comput. Phys.* **171**, 151. DOI. ADS.

Banerjee, D., Krishna Prasad, S., Pant, V., McLaughlin, J.A., Antolin, P., Magyar, N., Ofman, L., Tian, H., Van Doorsselaere, T., De Moortel, I., Wang, T.J.: 2021, Magnetohydrodynamic Waves in Open Coronal Structures. *Space Sci. Rev.* **217**, 76. DOI. ADS.

Berghmans, D., Clette, F.: 1999, Active region EUV transient brightenings - First Results by EIT of SOHO JOP 80. *Solar Phys.* **186**, 207. DOI. ADS.

Botha, G.J.J., Arber, T.D., Nakariakov, V.M., Zhugzhda, Y.D.: 2011, Chromospheric Resonances above Sunspot Umbrae. *Astrophys. J.* **728**, 84. DOI. ADS.

Brooks, D.H., Warren, H.P., Ugarte-Urra, I.: 2012, Solar Coronal Loops Resolved by Hinode and the Solar Dynamics Observatory. *Astrophys. J. Lett.* **755**, L33. DOI. ADS.

Cooper, F.C., Nakariakov, V.M., Tsiklauri, D.: 2003, Line-of-sight effects on observability of kink and sausage modes in coronal structures with imaging telescopes. *Astron. Astrophys.* **397**, 765. DOI. ADS.

De Moortel, I., Bradshaw, S.J.: 2008, Forward Modelling of Coronal Intensity Perturbations. *Solar Phys.* **252**, 101. DOI. ADS.

De Moortel, I., Hood, A.W.: 2003, The damping of slow MHD waves in solar coronal magnetic fields. *Astron. Astrophys.* **408**, 755. DOI. ADS.

De Moortel, I., Hood, A.W.: 2004, The damping of slow MHD waves in solar coronal magnetic fields. II. The effect of gravitational stratification and field line divergence. *Astron. Astrophys.* **415**, 705. DOI. ADS.

De Moortel, I., Ireland, J., Walsh, R.W., Hood, A.W.: 2002a, Longitudinal intensity oscillations in coronal loops observed with TRACE I. Overview of Measured Parameters. *Solar Phys.* **209**, 61. DOI. ADS.

De Moortel, I., Ireland, J., Hood, A.W., Walsh, R.W.: 2002b, The detection of 3 & 5 min period oscillations in coronal loops. *Astron. Astrophys.* **387**, L13. DOI. ADS.

DeForest, C.E., Gurman, J.B.: 1998, Observation of Quasi-periodic Compressive Waves in Solar Polar Plumes. *Astrophys. J. Lett.* **501**, L217. DOI. ADS.

Edwin, P.M., Roberts, B.: 1983, Wave Propagation in a Magnetic Cylinder. *Solar Phys.* **88**, 179. DOI. ADS.

Edwin, P.M., Roberts, B.: 1988, Employing analogies for ducted MHD waves in dense coronal structures. *Astron. Astrophys.* **192**, 343. ADS.

Freeland, S.L., Handy, B.N.: 1998, Data Analysis with the SolarSoft System. *Solar Phys.* **182**, 497. DOI. ADS.

Goedbloed, J.P.H., Poedts, S.: 2004, *Principles of Magnetohydrodynamics*, Cambridge University Press, Cambridge. ADS.

Heyvaerts, J., Priest, E.R.: 1983, Coronal heating by phase-mixed shear Alfven waves. *Astron. Astrophys.* **117**, 220. ADS.

Kobanov, N., Kolobov, D., Chelpanov, A.: 2015, Oscillations Above Sunspots and Faculae: Height Stratification and Relation to Coronal Fan Structure. *Solar Phys.* **290**, 363. DOI. ADS.

Kolotkov, D.Y., Nakariakov, V.M., Zavershinskii, D.I.: 2019, Damping of slow magnetoacoustic oscillations by the misbalance between heating and cooling processes in the solar corona. *Astron. Astrophys.* **628**, A133. DOI. ADS.

Krishna Prasad, S., Banerjee, D., Van Doorsselaere, T.: 2014, Frequency-dependent Damping in Propagating Slow Magneto-acoustic Waves. *Astrophys. J.* **789**, 118. DOI. ADS.

Krishna Prasad, S., Jess, D.B., Van Doorsselaere, T.: 2019, The temperature-dependent damping of propagating slow magnetoacoustic waves. *Front. Astron. Space Sci.* **6**, 57. DOI. ADS.

Krishna Prasad, S., Banerjee, D., Van Doorsselaere, T., Singh, J.: 2012, Omnipresent long-period intensity oscillations in open coronal structures. *Astron. Astrophys.* **546**, A50. DOI. ADS.

Kumar, P., Innes, D.E., Inhester, B.: 2013, Solar Dynamics Observatory/Atmospheric Imaging Assembly Observations of a Reflecting Longitudinal Wave in a Coronal Loop. *Astrophys. J. Lett.* **779**, L7. DOI. ADS.

Li, B., Guo, M., Yu, H., Chen, S.-X., Shi, M.: 2023, Three-dimensional propagation of kink wave trains in solar coronal slabs. *Mon. Not. Roy. Astron. Soc.* **518**, L57. DOI. ADS.

Mandal, S., Krishna Prasad, S., Banerjee, D.: 2018, A Statistical Study on the Frequency-dependent Damping of the Slow-mode Waves in Polar Plumes and Interplumes. *Astrophys. J.* **853**, 134. DOI. ADS.

Mandal, S., Magyar, N., Yuan, D., Van Doorsselaere, T., Banerjee, D.: 2016, Forward Modeling of Propagating Slow Waves in Coronal Loops and Their Frequency-dependent Damping. *Astrophys. J.* **820**, 13. DOI. ADS.

Marsh, M.S., De Moortel, I., Walsh, R.W.: 2011, Observed Damping of the Slow Magnetoacoustic Mode. *Astrophys. J.* **734**, 81. DOI. ADS.

Marsh, M.S., Walsh, R.W., De Moortel, I., Ireland, J.: 2003, Joint observations of propagating oscillations with SOHO/CDS and TRACE. *Astron. Astrophys.* **404**, L37. DOI. ADS.

Morgan, H., Habbal, S.R., Li, X.: 2004, Hydrogen Lyα Intensity Oscillations Observed by the Solar and Heliospheric Observatory Ultraviolet Coronagraph Spectrometer. *Astrophys. J.* **605**, 521. DOI. ADS.

Nakariakov, V.M.: 2006, Magnetohydrodynamic waves in coronal polar plumes. *Phil. Trans. Roy. Soc. A* **364**, 473. DOI. ADS.

Nakariakov, V.M., Kolotkov, D.Y.: 2020, Magnetohydrodynamic Waves in the Solar Corona. *Annu. Rev. Astron. Astrophys.* **58**, 441. DOI. ADS.

Nakariakov, V.M., Zimovets, I.V.: 2011, Slow Magnetoacoustic Waves in Two-ribbon Flares. *Astrophys. J. Lett.* **730**, L27. DOI. ADS.

Nakariakov, V.M., Verwichte, E., Berghmans, D., Robbrecht, E.: 2000, Slow magnetoacoustic waves in coronal loops. *Astron. Astrophys.* **362**, 1151. ADS.

Nakariakov, V.M., Kosak, M.K., Kolotkov, D.Y., Anfinogentov, S.A., Kumar, P., Moon, Y.-J.: 2019, Properties of Slow Magnetoacoustic Oscillations of Solar Coronal Loops by Multi-instrumental Observations. *Astrophys. J. Lett.* **874**, L1. DOI. ADS.

Ofman, L., Nakariakov, V.M., DeForest, C.E.: 1999, Slow Magnetosonic Waves in Coronal Plumes. *Astrophys. J.* **514**, 441. DOI. ADS.

Ofman, L., Romoli, M., Poletto, G., Noci, G., Kohl, J.L.: 1997, Ultraviolet Coronagraph Spectrometer Observations of Density Fluctuations in the Solar Wind. *Astrophys. J. Lett.* **491**, L111. DOI. ADS.

Owen, N.R., De Moortel, I., Hood, A.W.: 2009, Forward modelling to determine the observational signatures of propagating slow waves for TRACE, SoHO/CDS, and Hinode/EIS. *Astron. Astrophys.* **494**, 339. DOI. ADS.

Pascoe, D.J., Nakariakov, V.M., Kupriyanova, E.G.: 2014, Fast magnetoacoustic wave trains in coronal holes. *Astron. Astrophys.* **568**, A20. DOI. ADS.

Roberts, B.: 1981, Wave Propagation in a Magnetically Structured Atmosphere - Part Two - Waves in a Magnetic Slab. *Solar Phys.* **69**, 39. DOI. ADS.

Roberts, B., Webb, A.R.: 1978, Vertical motions in an intense magnetic flux tube. *Solar Phys.* **56**, 5. DOI. ADS.

Schmelz, J.T., Christian, G.M., Chastain, R.A.: 2016, The Coronal Loop Inventory Project: Expanded Analysis and Results. *Astrophys. J.* **831**, 199. DOI. ADS.

Selwa, M., Murawski, K., Solanki, S.K.: 2005, Excitation and damping of slow magnetosonic standing waves in a solar coronal loop. *Astron. Astrophys.* **436**, 701. DOI. ADS.

Su, J.T.: 2014, Statistical Detection of Slow-mode Waves in Solar Polar Regions with SDO/AIA. *Astrophys. J.* **793**, 117. DOI. ADS.

Sych, R., Nakariakov, V.M., Karlicky, M., Anfinogentov, S.: 2009, Relationship between wave processes in sunspots and quasi-periodic pulsations in active region flares. *Astron. Astrophys.* **505**, 791. DOI. ADS.

Van Doorsselaere, T., Brady, C.S., Verwichte, E., Nakariakov, V.M.: 2008, Seismological demonstration of perpendicular density structuring in the solar corona. *Astron. Astrophys.* **491**, L9. DOI. ADS.

Van Doorsselaere, T., Antolin, P., Yuan, D., Reznikova, V., Magyar, N.: 2016, Forward modelling of optically thin coronal plasma with the FoMo tool. *Front. Astron. Space Sci.* **3**, 4. DOI. ADS.

Verwichte, E., Marsh, M., Foullon, C., Van Doorsselaere, T., De Moortel, I., Hood, A.W., Nakariakov, V.M.: 2010, Periodic Spectral Line Asymmetries in Solar Coronal Structures from Slow Magnetoacoustic Waves. *Astrophys. J. Lett.* **724**, L194. DOI. ADS.

Voitenko, Y., Andries, J., Copil, P.D., Goossens, M.: 2005, Damping of phase-mixed slow magneto-acoustic waves: Real or apparent? *Astron. Astrophys.* **437**, L47. DOI. ADS.

Wang, T.J., Ofman, L., Davila, J.M., Mariska, J.T.: 2009, Hinode/EIS observations of propagating low-frequency slow magnetoacoustic waves in fan-like coronal loops. *Astron. Astrophys.* **503**, L25. DOI. ADS.

Wang, T., Ofman, L., Yuan, D., Reale, F., Kolotkov, D.Y., Srivastava, A.K.: 2021, Slow-Mode Magnetoacoustic Waves in Coronal Loops. *Space Sci. Rev.* **217**, 34. DOI. ADS.

Williams, T., Walsh, R.W., Regnier, S., Johnston, C.D.: 2021, Multi-Stranded Coronal Loops: Quantifying Strand Number and Heating Frequency from Simulated Solar Dynamics Observatory (SDO) Atmospheric Imaging Assembly (AIA) Observations. *Solar Phys.* **296**, 102. DOI. ADS.

Zhugzhda, Y.D.: 1996, Force-free thin flux tubes: Basic equations and stability. *Phys. Plasmas* **3**, 10. DOI. ADS.

Zhugzhda, Y.D., Goossens, M.: 2001, Hidden problems of thin-flux-tube approximation. *Astron. Astrophys.* **377**, 330. DOI. ADS.